# Time-resolved X-ray study of poly(aryl ether ether ketone) crystallization and melting behaviour: 1. Crystallization

**Benjamin S. Hsiao*†, KennCorwin H. Gardner‡ and Dan Q. Wu§**
*DuPont Company, Experimental Station, Wilmington, DE 19880, USA*

**and Benjamin Chu**
*Department of Chemistry, State University of New York at Stony Brook, Long Island, NY 11794-3400, USA*
*(Received 22 January 1993)*

Time-resolved simultaneous small-angle X-ray scattering (SAXS) and wide-angle X-ray diffraction (WAXD) experiments using synchrotron radiation were made in order to study the isothermal crystallization behaviour of poly(aryl ether ether ketone) (PEEK). Two types of long period ($L_B$ and $L_C^M$), the scattering invariant $Q$, and the linear degree of crystallinity within the lamellar stacks $x_{CL}$ were estimated from the Lorentz-corrected plot and the correlation function. As a result, the average lamellar thickness $l_C$ was calculated as the product of $L_C^M$ and $x_{CL}$ during crystallization at temperatures of 230–310°C. The bulk degree of crystallinity (by weight), $\psi_C$, was determined by WAXD. It was found that both long periods decreased, $Q$ increased and $l_C$ remained approximately constant with time. The decrease in the long period was explained by the lamellar insertion within the lamellar stacks, whereas the increase in $Q$ was attributed to the increase in the bulk-volume degree of crystallinity $x_C$, rather than $x_{CL}$. In addition, the values of the long period and of $Q$ were found to increase with temperature as a result of the thicker lamellae. Finally, our results support the model of two populations in lamellar thickness, namely the primary lamellae which are developed first in bundle-like stacks, and the narrower, secondary lamellae (as a small fraction) that are inserted later between the primary lamellae under various spatial restrictions.

**(Keywords: simultaneous SAXS/WAXD; crystallization; PEEK)**

## INTRODUCTION

Time-resolved synchrotron X-ray techniques have been shown to be useful in studying rapid structural changes in polymers. For example, the crystal structure and morphology of polyethylene[1,2], its blends (LDPE/HDPE)[3–5] and chain-folded single crystals[6] have been studied by small-angle X-ray scattering (SAXS) and wide-angle X-ray diffraction (WAXD) in real time. The experiments showed that the long period $L$, the invariant $Q$ and the lamellar thickness $l_C$ all increased with time and temperature. These results were attributed to the effect of lamellar thickening. Such time-resolved structural information is difficult to obtain by techniques such as electron microscopy and conventional X-ray scattering, because of complicated sample preparation and/or lengthy collection times. Recently, several simultaneous synchrotron techniques such as SAXS/WAXD/small-angle laser scattering (SALS)[7], SAXS/d.s.c.[8,9] and WAXD/d.s.c.[10] have been developed. These techniques have enhanced the uniqueness of using synchrotron X-rays to study phase transitions in polymers.

In this work, we have studied the crystallization and melting behaviour of poly(aryl ether ether ketone) (PEEK), using simultaneous SAXS/WAXD techniques. While the thermal properties[11–16] and morphological features[17–21] of PEEK are well characterized, there are unresolved questions concerning the crystallization and melting behaviour of PEEK that may be addressed by using time-resolved SAXS measurements. In this paper, we shall discuss isothermal crystallization studies of the quenched PEEK melts and the SAXS data analysis procedure. In a subsequent paper we will discuss a melting study of amorphous and isothermally crystallized PEEK samples.

The thermal properties of PEEK have been characterized by many laboratories[11–16]. PEEK is a semicrystalline polymer having a $T_g$ of 145°C, an equilibrium melting temperature $T_m^0$ of about 395°C and a maximum degree of crystallinity of about 40% (by weight, in the unoriented sample). The maximum crystallization rate was found to occur near 230°C[11,22,23]. Because crystallization rates in this region were too fast to be measured by thermal analysis[24], isothermal crystallization kinetics data are available only at temperatures above 290°C, and these data could not be fitted by a single-exponent Avrami equation[25,26]. This deviation implies that the crystallization process involved more than a single stage. For most polymers, two stages of crystallization are acknowledged[27]: a fast primary stage during which

* To whom correspondence should be addressed
† DuPont Fibers
‡ DuPont Central Research and Development
§ DuPont Polymers

0032-3861/93/193986-10
© 1993 Butterworth-Heinemann Ltd.

spherulite growth is linear, and a slow secondary stage which begins after spherulite impingement. Although the secondary stage is often attributed to the lamellar thickening or the growth of subsidiary lamellae within the spherulite, there is little information to reveal the correct mechanism.

PEEK has been observed to exhibit spherulitic growth when crystallized from the melt or the glassy state. However, recent optical microscopy on thin films made by Marand and Prasad[20] suggested that, at crystallization temperatures above 300°C, the spherulite morphology converts to 'crystal-aggregate-like' structures. Lovinger *et al.*[21] have used transmission electron microscopy (TEM) to investigate this phenomenon and concluded that the morphological changes at high crystallization temperatures (>300°C) were not due to polymorphism or a variation of lamellar growth habit, but instead were attributed to changes in lamellar thickness and stacking effects. They observed that, at crystallization temperatures below 300°C, the spherulites usually consisted of narrow lamellae which nucleated preferentially in contact with the substrate[18], whereas at temperatures above 300°C, the spherulites contained large, branched, bundle-like stacked lamellae, in addition to the narrow species[21]. The dual-lamellar thickness morphology in PEEK was first proposed by Bassett *et al.*[17], based on the TEM examination of replicas of etched surfaces from specimens crystallized at different temperatures. This morphology was also used to explain the double-melting behaviour observed in the d.s.c. studies. We feel that the time-resolved SAXS/WAXD technique is suitable for examining the lamellar morphology in *bulk samples* at different temperatures, in addition to testing the dual-thickness morphology model.

Morphological studies have shown that crystal structures are very heterogeneous during the crystallization process. Even when spherulite impingement begins, only part of the volume is occupied by the more or less regular lamellar stacking which contributes towards the SAXS maximum, if any. Consequently, the conventional approach[11,15] of using the long period $L$ (determined by the scattering maximum in SAXS) and the bulk degree of crystallinity $\psi_C$ (determined by WAXD) to estimate the lamellar thickness $l_C$ is unsuitable, because the assumption of an ideal two-phase model cannot be applied to the entire volume. Therefore, we have adopted a correlation-function method to extract the lamellar variables (i.e. long period $L$, scattering invariant $Q$, linear degree of crystallinity within the long period $x_{CL}$ and lamellar thickness $l_C$) from the SAXS data. This method has been discussed by Stroble and Schneider[28] and recently by Santa-Cruz *et al.*[29]. In addition, we measured the degree of crystallinity (in terms of weight fraction) by using the simultaneous WAXD technique.

## EXPERIMENTAL

### *Materials and preparation*

Commercially available PEEK (150G, from ICI) was used for all experiments; this polymer has a $T_g$ of 145°C and an approximate equilibrium melting temperature $T_m^0$ of 395°C[11]. The sample has a weight-average molecular weight $M_w$ of 38 000 and a number-average molecular weight $M_n$ of 14 000 (determined by g.p.c., using polystyrene standards). Powder samples were first moulded (from 400°C) into void-free amorphous discs (diameter 6.75 mm, thickness 1.1 mm), using a cold press quenching technique, for the synchrotron X-ray measurements. All samples were vacuum dried at 100°C for 24 h prior to the preparations or measurements.

### *Thermal analysis*

A Perkin-Elmer DSC-7 instrument was used to study the isothermal crystallization kinetics of PEEK. All samples were first equilibrated at 400°C for 5 min in order to eliminate any residual crystallinity. Two techniques were used to measure the crystallization isotherms. The first technique employed the cooling of the polymer melt, at a rate of 320°C min$^{-1}$, to the desired temperature (above 300°C), where the *melt* crystallization time was measured. The second technique involved the quenching of the melt using liquid nitrogen, followed by subsequent heating to the crystallization temperature (below 170°C), where the *cold* crystallization time was measured. The crystallization peak time was recorded at the maximum exothermic heat flow. No measurement was made between 170°C and 300°C, because the crystallization rate in this temperature range was too fast to be accurately determined by d.s.c.

### *Time-resolved X-ray measurements*

Simultaneous SAXS and WAXD measurements were performed at the X3A2 SUNY beamline, National Synchrotron Light Source, Brookhaven National Laboratory ($\lambda = 0.154$ nm). A dual-chamber temperature-jump device[3], capable of operating at temperatures up to 450°C, was constructed for this work (*Figure 1*). The SAXS data were collected using modified Kratky optics[30] (beam size = $1.5 \times 0.2$ mm$^2$, sample–detector distance = 50 cm) and a linear position sensitive detector (EG and G, PARC, Model 1453). The WAXD data were measured by a second linear position sensitive detector (Braun). WAXD data were only collected in the angular range where $2\theta = 21.0$–$35.5°$, due to spatial limitations.

Samples were initially equilibrated at 400°C ($T_1$) for 5 min, then jumped (using a pneumatic piston) to a lower crystallization temperature ($T_2$). During the initial 90% temperature drop ($\Delta T = T_1 - T_2$), the cooling rate was approximately 300°C min$^{-1}$. A time of 5–30 s was needed for the sample to reach $T_2$, depending on the degree of supercooling. The data collection time was chosen to be from 3 to 10 s. Longer data collection times were used when studying the lower degree of supercooling (or higher crystallization temperature). In total, nine crystallization temperatures were investigated (230–310°C, in intervals of 10°C).

All SAXS signals were corrected for absorption, background and incident beam fluctuation after a

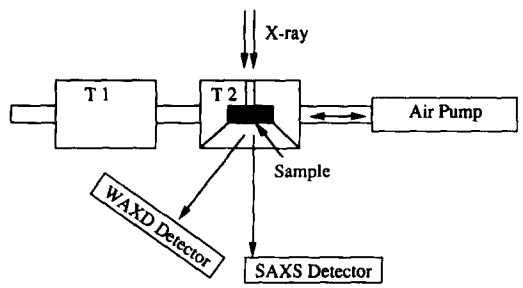


**Figure 1** Simultaneous SAXS and WAXD experimental set-up using a dual-chamber temperature-jump apparatus

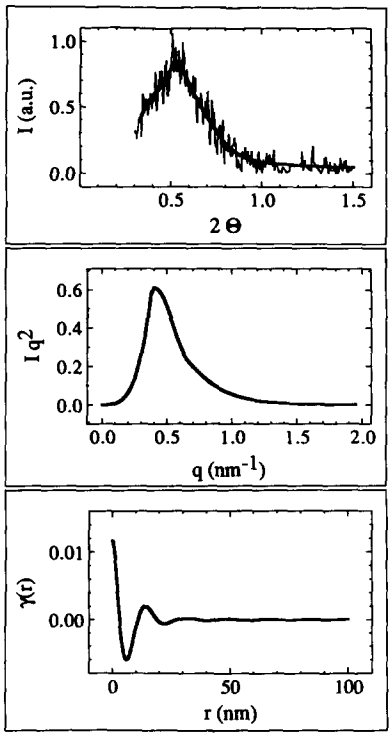


**Figure 2** Data analysis procedures for smoothing the as-measured SAXS signals. The top diagram represents the filtering process using a low-frequency band-pass filtering subroutine, the middle diagram is the Lorentz plot of the smoothed data (after the $I_b$ subtraction and extrapolation of the intensity to $q=0$ and $\infty$), while the bottom diagram is the Fourier transform of the smoothed data

smoothing procedure had been followed (*Figure 2*). A band pass filter was used to eliminate the high frequency noise (comprising 99% of the frequency distribution) of the scattering signals. The filtered signals were then fit with a cubic spline function (top curve, *Figure 2*). The recovered data were used for the Lorentz corrected plot ($I_q^2$ vs. $q$, where $q=4\pi\sin(\theta)/\lambda$) (middle curve, *Figure 2*), with the intensity extrapolated to $q=0$ and $\infty$ (which will be discussed below), and the Fourier transformation ($\gamma(r)$ vs. $r$) (bottom curve, *Figure 2*). For the simultaneous WAXD analysis, the diffraction pattern from a non-crystalline sample was scaled and subtracted from the semicrystalline pattern. The crystallinity index is defined as the ratio of the area under the residual pattern divided by the total scattering in the original pattern. The recovered crystalline samples (after the synchrotron measurements) were also calibrated by a Philips diffractometer and by d.s.c. to determine the bulk degree of crystallinity $\psi_C$.

*SAXS analysis*

Although Kratky optics were used, the small slit-length/width ratio and the long sample–detector distance, combined with the virtually parallel incident synchrotron beam, tends to minimize any smearing effects. Consequently, no desmearing procedure was applied to the scattering data, and they were treated as if generated using pin-hole collimation.

*Correlation function.* In *Figure 2* (top curve), the scattering intensity fall-off (after the maximum) covers a large angular range (i.e. $2\theta=0.5$–$1.5°$). The correlation function $\gamma(r)$ can be taken directly as the Fourier transform of the scattering intensity $I(q)$ (even without the correction of the truncation effects at high values of $q$) after the subtraction of the local electron-density fluctuation $I_b$ (assumed constant over the measured angular range). The contribution of $I_b$ was estimated by using Porod's law[31]:

$$I(q)=I_b+Kq^{-4} \tag{1}$$

which assumed a sharp interface between the two phases. Equation (1) indicates that we can plot $I(q)q^4$ against $q^4$ and extrapolate a straight line in the high-$q$ region (*Figure 3*). The intercept of this line was $K$ (Porod's asymptote) and the slope represented the degree of local electron-density fluctuation $I_b$.

We have further corrected truncation effects at both low and high values of $q$ to calculate $\gamma(r)$ with better precision. The value of $K$ was used to extrapolate the intensity ($=Kq^{-4}$) to $q=\infty$, and the value of $I(q_1)$ was used to extrapolate the intensity to $q=0$ (assuming a straight-line relationship between $[I(q_1)-I_b]q_1^2$ and 0, where $q_1$ is the lower limit of the SAXS measurement)[32]. Thus the correlation function can be written as:

$$\gamma(r)=(1/2\pi^2)\int_0^\infty (I(q)-I_b)q^2\cos(qr)\,dq \tag{2}$$

This equation represents the three-dimensional correlation function of the unoriented system. No finite phase boundary thickness correction was included in the analysis of $\gamma(r)$.

Several of the variables relating to lamellar morphology were estimated from $\gamma(r)$. The approach is illustrated in *Figure 4*, which shows a typical correlation function measured at 310°C. The deviation from linear behaviour when $r$ approaches zero indicates the presence of a diffuse boundary. This deviation is expected, since no finite phase boundary thickness correction was made. Therefore, the straight-line fit to $r=0$ yields the value of $Q$ (the invariant)[28]. Two long-period values can be determined here: the position of the first maximum, designated as $L_C^M$, and twice the value of the first minimum, designated as $L_C^m$ (using the notations of Santa-Cruz *et al.*[29]). These two values do not usually coincide in our study, which indicates that we are not dealing here with an ideal two-phase system. In addition to the long period, the linear degree of crystallinity ($x_{CL}$) within the lamellar stacks, can be determined from $\gamma(r)$. The following equation was used for this purpose:

$$x_1x_2L_C^M=B \tag{3}$$

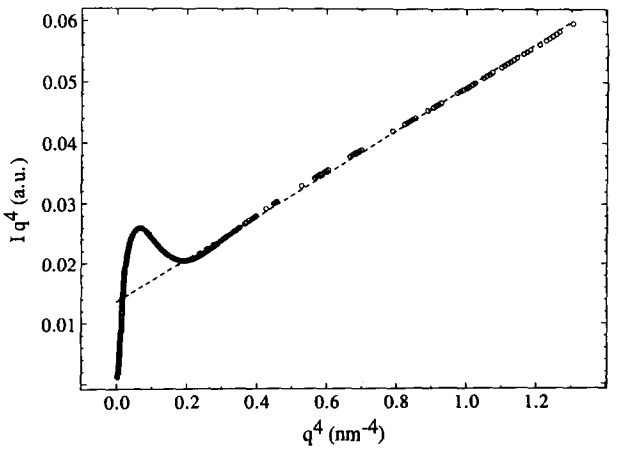


**Figure 3** Porod plot to extrapolate the local electron-density fluctuation $I_b$; the non-equal spacing was a result of the smoothing procedure

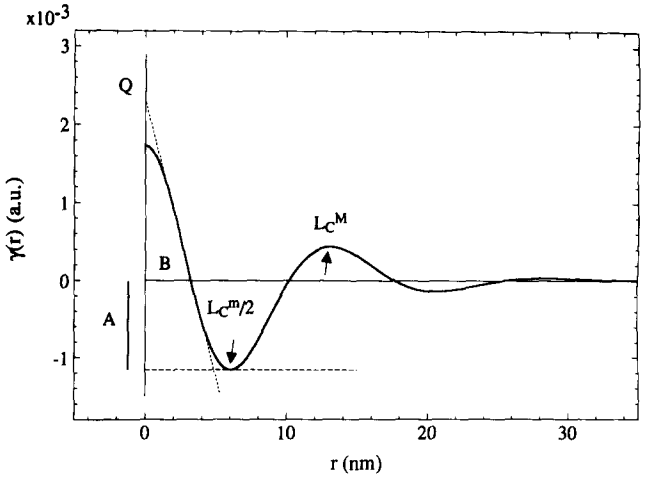


**Figure 4** A typical correlation function, $\gamma(r)$, derived from the corrected intensity; this does not include any correction for finite interface thickness

where $x_1$ and $x_2$ represent the volume fractions of the components of phases 1 and 2 within the two-phase stacks ($x_1 + x_2 = 1$), and $B$ is the first intercept with the ($\gamma(r) = 0$) line. Equation (3) does not reveal which value (i.e. $x_1$ or $x_2$) represents the linear degree of crystallinity $x_{CL}$. The proper assignment of each fraction has to be determined in conjunction with the bulk-volume degree of crystallinity $x_C$ (determined from $\psi_C$ after the density conversion). The lamellar thickness $l_C$ was then calculated as the product of $L_C^M$ and $x_{CL}$.

## RESULTS

The isothermal crystallization peak time for PEEK measured by d.s.c. is shown in *Figure 5*. The crystallization peak time was used instead of the crystallization half-time because of difficulties in defining the initial heat-flow base line at some of the crystallization temperatures. This occurs during the temperature transition from the cooling to the isothermal mode, if the crystallization rate is too fast[26]. Although the crystallization peak time is usually smaller than the crystallization half-time, it is also inversely proportional to the crystallization rate. In *Figure 5*, the dotted line represents a second-order polynomial fit to the experimental peak times. Although the physical significance of this fit is only minimal, the estimated maximum crystallization rate temperature is approximately 230°C and is in agreement with published results[11]. We have used this plot to aid us in selecting suitable data collection times for time-resolved X-ray measurements. When the crystallization temperature is above 300°C, the peak time is greater than 30 s (the maximum time needed for the sample to equilibrate at $T_2$). Consequently, the scattering maximum occurs at times greater than what are required to reach temperature equilibrium and the scattering data were collected under isothermal conditions. In contrast, when the crystallization temperature is lower than 300°C, the peak time is shorter than 30 s and the possibility exists that the initial scattering data were collected during the temperature transition stage. To eliminate the possibility of treating non-isothermal data, scattering data collected at times less than 30 s were discarded.

Two examples of selected unsmoothed time-resolved SAXS patterns ($I$ vs. detector pixel) for PEEK crystallized at 230°C and 310°C (after the correction of absorption, background and incident beam fluctuation) are shown in *Figures 6a* and *6b*, respectively. The data collection time was 3 s for the measurements made at 230°C and 10 s for those made at 310°C (consequently a better signal/noise ratio was observed). In the 230°C measurement, some SAXS profiles appeared at times before 30 s, and as these results were probably under non-isothermal conditions they were discarded for further analysis. In contrast, in the 310°C measurement, all the

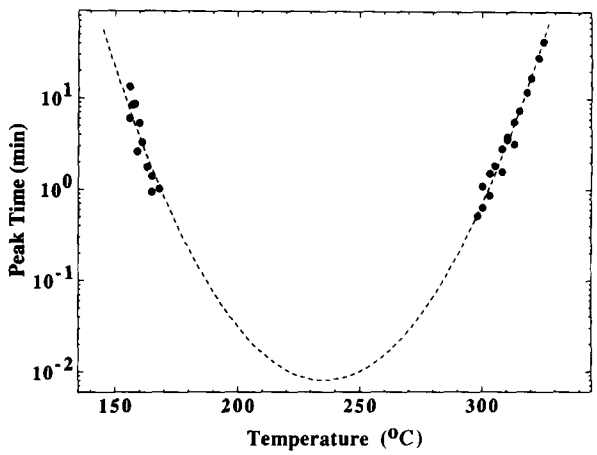


**Figure 5** Isothermal crystallization peak time plot for PEEK determined by d.s.c., in which the dotted line represents an extrapolation using a second-order polynomial fit

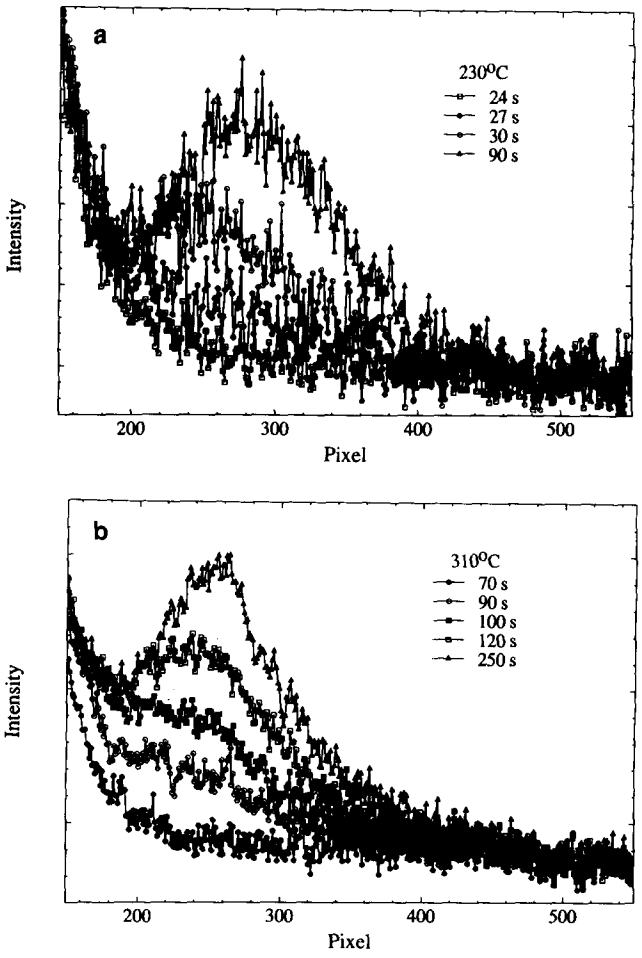


**Figure 6** Selected unsmoothed SAXS patterns measured for PEEK at: (a) 230°C (collection time = 3 s) and; (b) 310°C (collection time = 10 s). The angular values increase with the pixel number, with the centre of the beam located at the 84 pixel; intensities are in arbitrary units

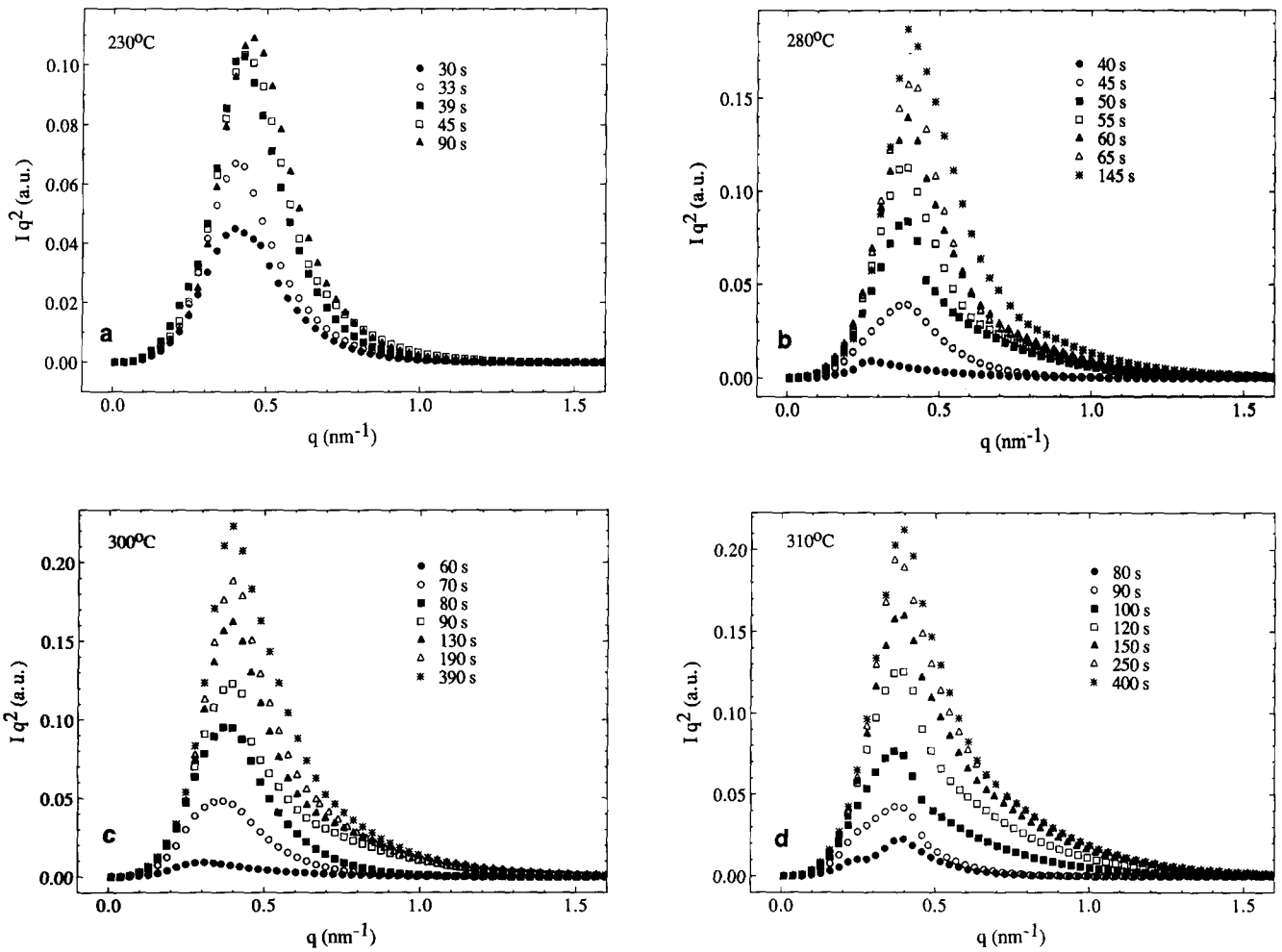


**Figure 7** Selected time-resolved Lorentz-corrected SAXS patterns (after smoothing) of PEEK crystallization recorded under the following conditions: (a) 230°C (collection time = 3 s); (b) 280°C (5 s); (c) 300°C (10 s) and; (d) 310°C (10 s)

SAXS profiles appeared after 30 s and thus were considered as being under isothermal conditions. In these two plots, the intensity maximum is seen to increase in magnitude and shift to a higher angle (a higher pixel value) at longer times. Lorentz-corrected plots of the corresponding smoothed patterns, $(I-I_b)\ q^2$ vs. $q$, abbreviated to $I_q^2$ vs. $q$, were generated for samples isothermally crystallized at four selected temperatures (230, 280, 300 and 310°C) (*Figures 7a–d*). The data collection times in these figures, ranging from 3 to 10 s, were chosen based on the crystallization rates. At higher degrees of supercooling (230–270°C), the fast crystallization rate necessitated a data collection time of 3 s intervals, while at lower degrees of supercooling (290–310°C), the slower crystallization rate allowed a collection time of 10 s. For all crystallization conditions, peak position ($q_{max}$) and peak area (proportional to the invariant $Q$) were observed to increase with increasing crystallization time. At 310°C, the initial SAXS profile (80 s) exhibits a weak secondary shoulder at a low value of $q$. The position of this shoulder was similar to the value of $q_{max}$ in the initial profile of the 280°C (40 s) and 300°C (60 s) measurements.

The long period, an average distance between two adjacent lamellae, was calculated from $q_{max}$ by using Bragg's law ($L_B = 2\pi/q_{max}$). A plot of $L_B$ vs. time for different crystallization temperatures is shown in *Figure 8*. In this plot, the spatial resolution for $q_{max}$ was poor, which was attributed to the reduction in data points after the smoothing procedure. A general trend of the decrease in $L_B$ with time was observed. It was found that $L_B$ decreased significantly in value during the initial crystallization stage and then gradually levelled off at the later crystallization stage for all of the crystallization temperatures. The final value of the long period was found to increase with crystallization temperature, e.g. the final value of $L_B$ at 230°C was 14.7 nm, and at 310°C was 15.9 nm.

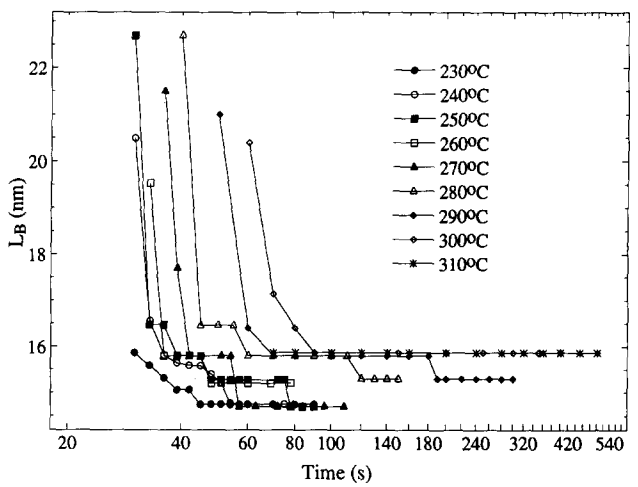


**Figure 8** Variation in the long period $L_B$ (determined from the scattering maxima in *Figure 7* using Bragg's law) with time, for PEEK crystallization at different temperatures

Selected corresponding correlation functions $\gamma(r)$, derived from data collected at 230 and 310°C, are shown in *Figures 9a* and *9b*, respectively. The correlation functions were calculated from the data displayed in *Figure 7*, by using equation (2), and were used to determine the lamellar variables $L_C^M$, $x_{CL}$ and $Q$. The long period $L_C^M$ is defined as the position of the first maximum in $\gamma(r)$. In *Figures 9a* and *9b*, $L_C^M$ is observed to decrease with increasing crystallization time. The values of $L_C^M$, measured at different times and temperatures (see *Figure 10*), show a trend similar to that observed in $L_B$ (see *Figure 8*). However, $L_C^M$ is approximately 1 nm smaller than $L_B$ and appears to have a better resolution. For example, no difference was observed between the final values of $L_B$ at 300 and 310°C, but $L_C^M$ is clearly larger at 310°C than at 300°C. The second variable determined from $\gamma(r)$, i.e. the linear degree of crystallinity $x_{CL}$, could not be directly measured. Instead, the linear fraction within the lamellar stacks, $x_1$, was calculated from $\gamma(r)$ by using equation (3). Since $L_C^M$ decreased with time and the intercept value $B$ remained approximately constant (see *Figure 9*), the value of $x_1$ could either increase or decrease with time, according to equation (3). If $x_1$ decreases with time and it represents $x_{CL}$, then the initial lamellar thickness (as the product of $L_C^M$ and $x_{CL}$) will be very large and has to decrease significantly with further crystallization, suggesting a model that does not make physical sense. Therefore, $x_{CL}$ must increase with time. The values of $x_{CL}$ determined by this method are shown

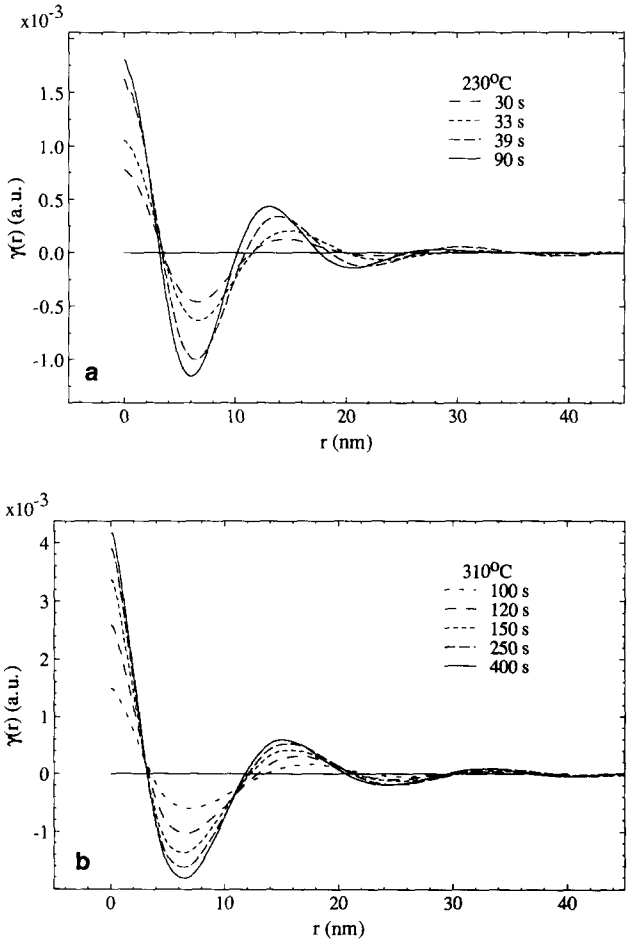


**Figure 9** The correlation function $\gamma(r)$ of the scattering data obtained for PEEK at (a) 230°C, and (b) 310°C, recorded at different crystallization times

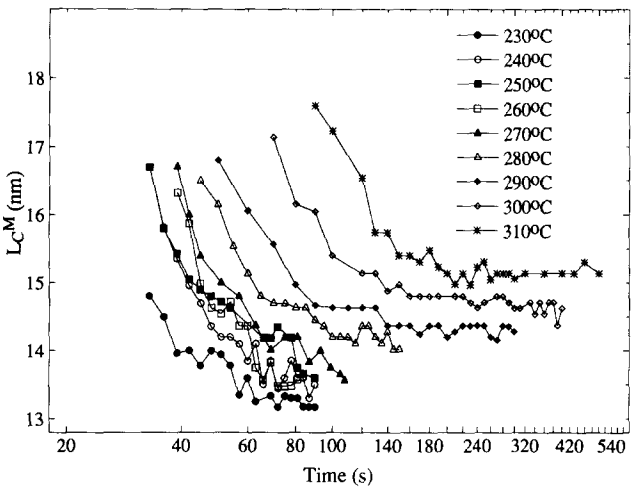


**Figure 10** Variation in the long period $L_C^M$ (determined from $\gamma(r)$) with time, for PEEK crystallization at different temperatures

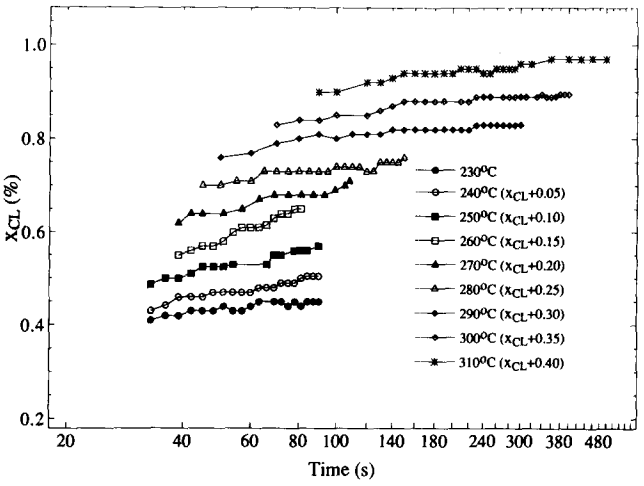


**Figure 11** Variation in the linear degree of crystallinity $x_{CL}$ (determined from $\gamma(r)$) with time, for PEEK crystallization at different temperatures; values are vertically shifted, as indicated, for better visualization

in *Figure 11* ($x_{CL}$ for the different temperatures are shifted vertically to avoid any overlap). The value of $x_{CL}$ was also found to increase with temperature, covering a range of 40–60%. The invariant $Q$, determined from the intercept of $\gamma(0)$, for different crystallization times and temperatures, is shown in *Figure 12*. $Q$ was observed to increase with both time and temperature. The shape of these $Q$ curves was similar to that observed for the degree of crystallinity changes during the crystallization measured by d.s.c.[13,14,25,26].

Selected WAXD patterns (in this case, at a crystallization temperature of 310°C), which were collected simultaneously with the previously described SAXS data, are shown in *Figure 13a*. Within the limited angular range ($2\theta = 21.0$–$35.5°$), two crystal peaks are observed which can be indexed as 200 and 211 reflections. The complete WAXD pattern ($2\theta = 4$–$50°$) is shown in *Figure 13b*. A crystallinity index for the partial WAXD pattern was determined by deconvoluting the measured patterns into crystalline and non-crystalline components, after background subtraction. The degree of crystallinity ($\psi_c$, as a weight fraction) was then estimated by scaling the crystallinity index using a well-crystallized PEEK sample as the calibration standard (characterized by conventional WAXD over a full angular range and by d.s.c. after the

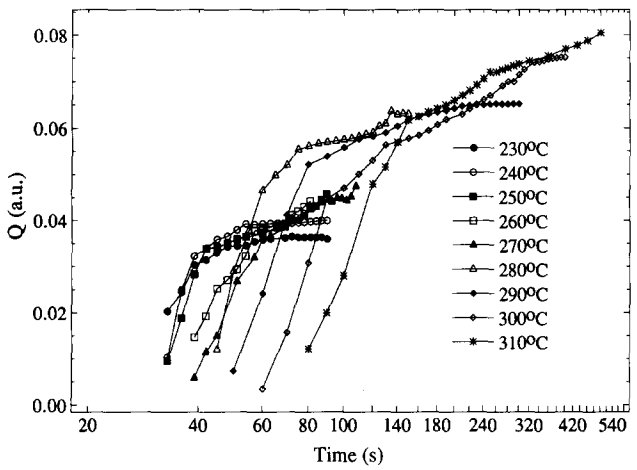


**Figure 12** Variation in the scattering invariant $Q$ (determined from *Figure 9*) with time, for PEEK crystallization at different temperatures

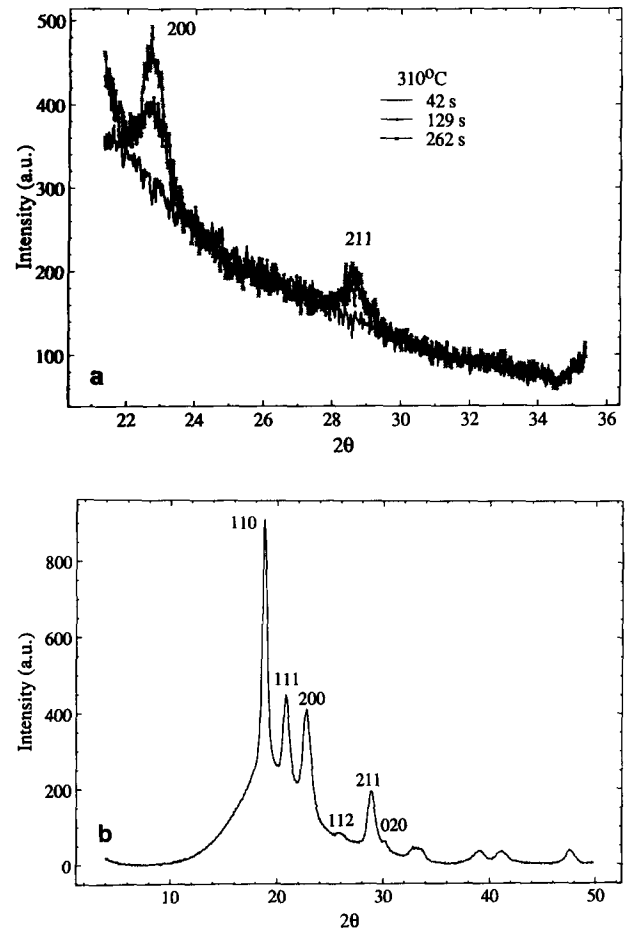


**Figure 13** (a) Simultaneous time-resolved WAXD patterns of PEEK samples crystallized at 310°C (collection time is ~40 s) and; (b) full WAXD pattern of crystalline PEEK

synchrotron measurement). The collection time for each synchrotron WAXD pattern was approximately 40 s. The change in crystallinity, as measured by simultaneous WAXD at three different crystallization temperatures (290–310°C), is shown in *Figure 14*. The 40 s collection time was too long to characterize the rapid crystallization at temperatures below 290°C. The maximum degree of crystallinity determined by simultaneous WAXD was about 35%, a value consistent with typical values derived from d.s.c. measurements.

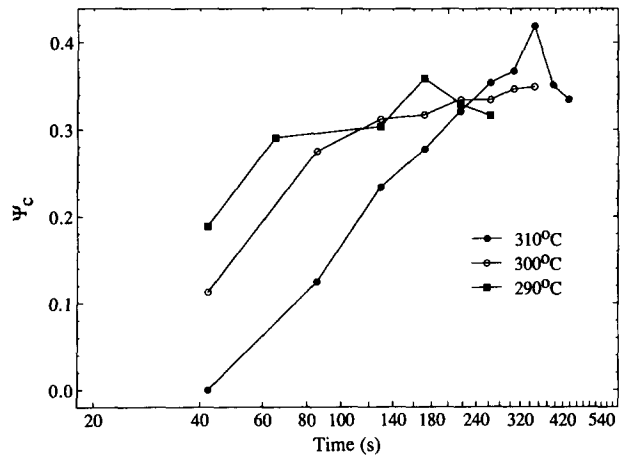


**Figure 14** Variation in the degree of crystallinity $\psi_c$ (weight fraction) with time, determined by WAXD at temperatures of 290, 300 and 310°C

## DISCUSSION

For the temperature-jump measurements, samples were quenched from a high temperature to low temperatures, with the maximum time to reach the measurement temperatures being approximately 30 s. D.s.c. measurements suggest that, within this time period, crystallization should have taken place at numerous crystallization temperatures (230–290°C) before isothermal conditions were reached. However, presumably because of the larger sample masses, longer crystallization induction times were found in the SAXS measurements than were observed by d.s.c. Only at high crystallization temperatures (i.e. 300 and 310°C) was a good agreement between the SAXS and d.s.c. measurements observed. Since the samples were reduced from a low-degree-of-supercooling state at a higher temperature (slower crystallization rate) to a high-degree-of-supercooling state at a lower temperature (faster crystallization rate), we feel that the data collected after the transient time are still indicative of isothermal crystallization.

In *Figures 8* and *10*, the $L_B$ and $L_C^M$ values were both found to decrease rapidly in the initial stage and then to gradually level off, and this behaviour was consistent over all of the crystallization temperatures. One explanation was that the initial crystallization took place during cooling, which produced a larger long period, and the later crystallization, occurring at lower temperatures, produced a smaller long period. In our experiment, this explanation is not acceptable because the decreases in $L$ at different crystallization temperatures should all begin at the same time if the initial crystallization took place during cooling. In addition, several measurements showed that $L$ fell at much later times than those needed to reach the measurement temperatures. Furthermore, a significantly longer time would be needed to induce crystallization above 310°C (for the 310°C measurement).

This decrease in the long period during crystallization has been previously observed by Zachmann and Schmidt in quenched samples of poly(ethylene terephthalate)[33], by Keller in the iso-PS system[34], by Nojima *et al.* in poly(ε-caprolactone)[35], by Zachmann in poly(ethylene naphthalene dicarboxylate)[36], and by Chu and co-workers in poly(aryl ether ketones)[37]. These observations suggest that a decrease in $L$ is a generic characteristic for semicrystalline polymers during the crystallization process. In the case of polyethylene, the long period has always been found to remain constant or increase with

the annealing time[6,36,38,39]. This may be because the interval during which $L$ decreases in polyethylene is simply too short to be detected. The increase in $L$(in the case of polyethylene) was attributed to the thickening of lamellae, which was observed in the later stage of the crystallization. In PEEK, the decrease in $L$ is not due to the thickening process, so another mechanism must be responsible for this behaviour.

Based on the observations of Bassett *et al.*[17] and Lovinger and co-workers[18,19,21], who showed that PEEK spherulites consist of bundle-like lamellar stacks, we used the following model to explain the decrease in $L$ during crystallization. It is conceivable that lamellar insertion may occur in some loosely stacked lamellar bundles within the spherulites (during and after the linear spherulite growth stage), which can lead to a decrease in the average long period. This mechanism is illustrated in *Figure 15* (left-hand diagram), and was originally proposed by Keller[34] to explain the reversible long period changes that were observed upon heating and cooling iso-PS. In addition, we speculate that the inserted lamellae may suffer from some spatial restrictions and result in a narrower thickness. In this model, we denote the initial lamellae as the primary lamellae and the inserted narrower lamellae as the secondary lamellae. Conceivably, the secondary lamellae may be produced either in the individual form (as shown in *Figure 15*) or in small bundles. In contrast, a densely stacked lamellar bundle (made of only the primary lamellae) with no insertion may also coexist in the spherulite, which is illustrated by the right-hand diagram in *Figure 15*. In this figure, the left dual-lamellar thickness model is similar to the one proposed by Bassett *et al.*[17], and will be the subject of a melting study using time-resolved SAXS, which will appear in a subsequent paper.

The decrease in $L$ with time can also be explained by the superposition of lamellae bundles having gradually changing long periods, but with no lamellar insertion taking place. This suggests that the initial lamellar stacking will be *loose* (thus giving a large long period)

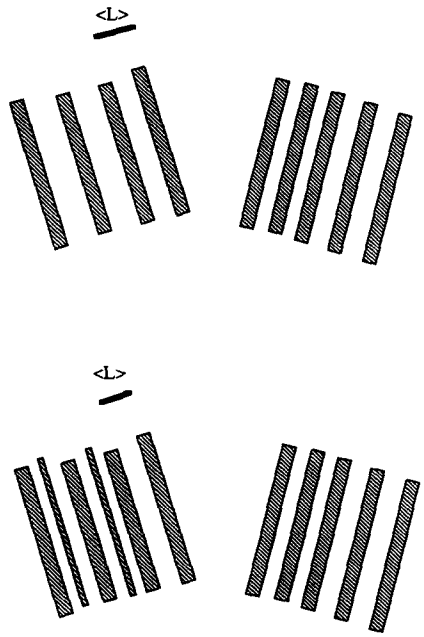


**Figure 15** Schematic representation of the lamellar insertion mechanism during crystallization; shaded bars represent the lamellae

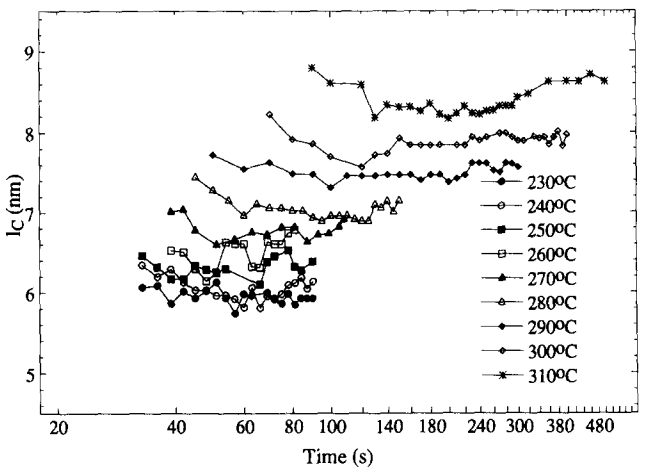


**Figure 16** Variation in the lamellar thickness $l_c$, calculated as the product of $L_C^M$ and $x_{CL}$, with time, for PEEK crystallization at different temperatures

and the later stacking will be *dense* (thus giving a small long period). However, such a lamellar arrangement is not consistent with TEM observations of the typical PEEK spherulite morphology[18–21]. Usually, the spherulite core contains more densely packed lamellar stacks than the outer perimeter region which leads us to believe that this is not a correct model.

The final values of $L_B$ (see *Figure 8*) were in good agreement with published results measured for quenched samples (crystallized at the same temperatures). For example, the $L_B$ value of 15.9 nm (at 310°C) in this present work is similar to the values of 15.7 nm, reported by Blundell and Osborn[11], and 14.8 nm found by Lee *et al.*[15]. The value of $L_B$ was found to be larger than that of $L_C^M$. This behaviour has also been observed by Santa-Cruz *et al.*[29] in PET, and was attributed to the broad distribution of lamellar thickness and long period. This is also true in the case of PEEK. In this material, the value of $L_C^M$ should be closer to the true value of the long period than $L_B$ is, and it may well be larger than this true value by some 20–50%, according to the work of Santa-Cruz *et al.*[29]. Using the values of $L_C^M$ and $x_{CL}$, the lamellar thickness $l_C$ was calculated (see *Figure 16*). It was found that $l_C$ remained somewhat constant throughout the crystallization, and there was no indication of lamellar thickening. As expected, the lamellar thickness was found to increase with the crystallization temperature, as a result of the lower degree of supercooling. This increase was consistent with the observation of an increase in the long period. In *Figure 16*, the values of $l_C$ ranged from 6 nm (230°C) to 9 nm (310°C); these values were probably larger than the actual values of the lamellar thickness. If these values were assumed to be overestimated by 30%[29], then the true values of $l_C$ would be in the range of 4 nm (at 230°C) to 6 nm (at 310°C).

In *Figure 12*, the scattering invariant $Q$ (in arbitrary units) was found to increase with time and temperature. Two separate models[29] were used to explain these results. The first model assumes that the invariant is linearly proportional to the volume fraction of the two-phase region. In this case, $Q$ can be written as:

$$Q = Cx_F x_{CL}(1 - x_{CL})(b_C - b_A)^2 \quad (4)$$

where $C$ is a calibration constant, $x_F$ (ranging from 0–1) is the volume fraction of the two-phase region and $b$ is

the electron-density contrast, i.e. $b_C$ and $b_A$, for the crystalline and amorphous components, respectively. Since the total volume degree of crystallinity $x_C$ is equivalent to the product of $x_F$ and $x_{CL}$, equation (4) thus becomes:

$$Q = Cx_C(1-x_{CL})(b_C-b_A)^2 \quad (5)$$

If the change in $x_{CL}$ is small (as in *Figure 11*), then $Q$ is dominated by the change in $x_C$ alone. Using the degree of crystallinity (as mass) $\psi_C$ [$=(x_C\rho_C)/\rho$, where $\rho$ is the density] measured by WAXD (*Figure 14*), we concluded that this model is in agreement with our invariant results. For instance, at 310°C, the value of $Q$ increased by about four times from 90 to 400 s, which was consistent with the change in $\psi_C$ (0.1 to 0.4, a fourfold increase) for the same time zone (the change in $\rho_C/\rho$ was small). In addition, the ratio of $Q$ increased with temperature (0.06 to 0.08, from 290 to 310°C), which was also consistent with the change in $\psi_C$ over the same temperature range (0.3 to 0.4, from 290 to 310°C). Nevertheless, there were some discrepancies between the SAXS and WAXD data. For example, at 290°C and 300°C, the WAXD results showed that the values of $\psi_C$ at 40 s were already about 0.1 and 0.2, respectively, whereas the SAXS measurements showed no detectable values of $Q$ at 40 s.

The second model assumes that the lamellar stacks and the interstack amorphous region form a random distribution of the layer-like arrangement, which also contributes diffuse scattering intensity to the invariant. In this case, $Q$ is written as:

$$Q = Cx_C(1-x_C)(b_C-b_A)^2 \quad (6)$$

which is a function of the product $x_C(1-x_C)$. We found that, at 310°C, the change in value of $\psi_C(1-\psi_C)$ from 90 to 400 s was only 0.09 to 0.24. This increase (less than threefold) was smaller than the observed increase in $Q$. Although Santa-Cruz *et al.* demonstrated that this model was superior to the first one for the fully crystallized PET system, we found that the first model (equation (4)) is more suitable for describing PEEK during the crystallization process.

## CONCLUSIONS

In conclusion, the intense brightness of synchrotron radiation has enabled us to study the crystallization of PEEK in real time using simultaneous SAXS and WAXD techniques. We have determined two types of long period ($L_B$ and $L_C^M$) using the Lorentz-corrected plot and correlation function, respectively. It was found that both long periods showed a large decrease in the initial stage and gradually levelled off in the final stage. The decrease in the long period was explained by lamellar insertion within the loosely stacked lamellar bundles, which were composed of primary lamellae. We spectulated that the inserted lamellae (secondary lamellae) may suffer from some spatial restrictions which result in a narrower thickness. The value of $L_B$ was found to be larger than $L_C^M$, which was attributed to the broad distribution of both lamellar thickness and long period. The linear degree of crystallinity $x_{CL}$ was also determined from $\gamma(r)$ and had values in the range 0.4–0.6 (slightly increased with temperature). The lamellar thicknesses, calculated from the values of $L_C^M$ and $x_{CL}$, ranged from 6 to 9 nm at temperatures from 230 to 310°C, which may be overestimated by at least 30%. There was no indication of lamellar thickening during the crystallization. Therefore, the secondary crystallization may consist primarily of two separate infilling processes, namely the subsidiary lamellar bundle formation and the secondary lamellar insertion. Finally, the invariant increase during the crystallization is mainly attributed to the increase in bulk crystallinity, following the expression:

$$Q = Cx_C(1-x_{CL})(b_C-b_A)^2$$

## ACKNOWLEDGEMENTS

The authors wish to thank J. P. McKeown, J. E. Frieda and Y. J. Li for their assistance in the synchrotron experiments, and Dr M. Keating and R. M. Koveleski for the thermal analysis measurements. Discussions with Drs A. Biswas, S. Z. D. Cheng, H. Marand and R. M. Ikeda were helpful in the preparation of this work. Financial support (to BC) by the National Science Foundation (Polymers Program: DMR 8921968) is also gratefully acknowledged.

## REFERENCES

1 Clements, J., Zachmann, H. G. and Ward, I. M. *Polymer* 1988, **29**, 1929
2 Ungar, G. *Am. Chem. Soc. Div. Polym. Chem. Polym. Prepr.* 1990, **31**, 108
3 Song, H. H., Stein, R. S., Wu, D. Q., Ree, M., Phillips, J. C., LeGrand, A. and Chu, B. *Macromolecules* 1988, **21**, 1180
4 Stein, R. S. *Am. Chem. Soc. Div. Polym. Chem. Polym. Prepr.* 1990, **31**, 113
5 Song, H. H., Wu, D. Q., Chu, B., Satkowski, M., Ree, M., Stein, R. S. and Phillips, J. C. *Macromolecules* 1990, **23**, 2380
6 Spells, S. J. and Hill, M. J. *Polymer* 1991, **32**, 2716
7 Bark, M., Schulze, C. and Zachmann, H. G. *Am. Chem. Soc. Div. Polym. Chem. Polym. Prepr.* 1985, **23**, 1109
8 Russell, T. P. and Koberstein, J. T. *J. Polym. Sci., Polym. Phys. Edn* 1986, **19**, 714
9 Galambos, A. F. PhD Thesis, Princeton University, 1989
10 Ungar, G., Feijoo, J. L., Keller, A., Yourd, R. and Percec, V. *Macromolecules* 1990, **23**, 3411
11 Blundell, D. J. and Osborn, B. N. *Polymer* 1983, **24**, 953
12 Cheng, S. Z. D., Cao, M. Y. and Wunderlich, B. *Macromolecules* 1986, **19**, 1868
13 Cebe, P. and Hong, S. D. *Polymer* 1986, **27**, 1183
14 Lee, Y. and Porter, R. S. *Macromolecules* 1987, **20**, 1336
15 Lee, Y., Porter, R. S. and Lin, J. S. *Macromolecules* 1989, **22**, 1756
16 Lee, Y. and Porter, R. S. *Macromolecules* 1988, **21**, 2770
17 Bassett, D. C., Olley, R. H. and Al Raheil, I. A. M. *Polymer* 1988, **29**, 1945
18 Lovinger, A. J. and Davis, D. D. *J. Appl. Phys.* 1985, **58**, 2843
19 Lovinger, A. J. and Davis, D. D. *Macromolecules* 1986, **19**, 1861
20 Marand, H. and Prasad, A. *Macromolecules* 1992, **25**, 1731
21 Lovinger, A. J., Hudson, S. and Davis, D. D. *Macromolecules* 1992, **25**, 1752
22 Medellin-Rodriguez, F. and Phillips, P. J. *SPE-ANTEC* 1990, 1264
23 Hsiao, B. S. and Sauer, B. B. *J. Polym. Sci., Polym. Phys. Edn* 1993, **31**, 901
24 Seferis, J. C. *Polym. Compos.* 1986, **7**, 158
25 Velisaris, C. and Seferis, J. *Polym. Eng. Sci.* 1986, **26**, 1574
26 Hsiao, B. S., Chang, I. Y. and Sauer, B. B. *Polymer* 1991, **32**, 2799
27 Wunderlich, B. 'Macromolecular Physics', Academic, New York, 1976
28 Strobl, G. R. and Schneider, M. *J. Polym. Sci., Polym. Phys. Edn* 1980, **18**, 1340
29 Santa-Cruz, C., Stribeck, N., Zachmann, H. G. and Bálta Calleja, F. J. *Macromolecules* 1991, **24**, 5980
30 Chu, B., Wu, D. Q. and Howard, R. *Rev. Sci. Instrum.* 1989, **60**, 3224
31 Koberstein, J. J., Morra, B. and Stein, R. S. *J. Appl. Crystallogr.* 1980, **13**, 34

32 Russell, T. P. in 'Handbook on Synchrotron Radiation' (Eds G. Brown and D. E. Moncton), Vol. 3, Elsevier, New York, 1991, p. 379
33 Zachmann, H. G. and Schmidt, G. F. *Makromol. Chem.* 1962, **52**, 23
34 Keller, A. IUPAC Int. Symp., Macromol. Proc., Florence, 1980, p. 135
35 Nojima, S., Kato, K., Ono, M. and Ashida, T. *Macromolecules* 1992, **25**, 1922
36 Zachmann, H. G. in 'Crystallization of Polymers', NATO Advanced Research Workshop Proceedings, Kluwer, in press
37 Wang, J., Alvarez, M., Zhang, W., Wu, Z., Li, Y. and Chu, B. *Macromolecules* 1992, **25**, 6943
38 Fischer, E. W. and Schmidt, G. F. *Angew. Chem.* 1962, **74**, 551
39 Fischer, E. W. *Kolloid Z., Z. Polym.* 1969, **231**, 458